Performance of Instantaneous Frequency Rate Estimation Using High-Order Phase Function

Pu Wang, Hongbin Li, Igor Djurović, and Braham Himed, *Fellow, IEEE*

***Abstract*—The high-order phase function (HPF) is a useful tool to estimate the instantaneous frequency rate (IFR) of a signal with a polynomial phase. In this paper, the asymptotic bias and variance of the IFR estimate using the HPF are derived in closed-forms for the polynomial phase signal with an arbitrary order. The Cramér-Rao bounds (CRBs) for IFR estimation, in both exact and asymptotic forms, are obtained and compared with the asymptotic mean-square error (MSE) of the HPF-based IFR estimator. Simulations are provided to verify our theoretical results.**

***Index Terms*—Cramér–Rao bound (CRB), high-order phase function (HPF), polynomial-phase signals.**

I. Introduction

Polynomial phase structure has been widely used to model nonstationary signals appearing in radar, sonar, communications, and passive acoustic applications [1], [2]. A pth-order polynomial phase signal (PPS) is given by

$$s(t) = A\exp\{j\phi(t)\} = A\exp\left\{j\sum_{i=0}^{p} a_i t^i\right\} \tag{1}$$

where A is the constant amplitude, $\phi(t)$ is the instantaneous phase (IP), and $\{a_i\}_{i=0}^{p}$ are unknown phase parameters, respectively. While the instantaneous frequency (IF) is the first derivative of the IP, the instantaneous frequency rate (IFR) is defined as the second derivative of the IP [3], i.e.,

$$\Omega(t) = \frac{d^2\phi(t)}{dt^2} = \sum_{i=2}^{p} i(i-1)a_i t^{i-2} \tag{2}$$

where $\Omega(t)$ denotes the IFR of the signal in (1). When $p = 2$, i.e., a linear FM signal, the IFR reduces to the well known chirp-rate, i.e., $\Omega(t) = 2a_2$ [4]. In practice, the IFR could reveal the rate-of-change of the velocity, i.e., acceleration, of a moving target.

IFR estimation is a frequently encountered task in radar applications. In synthetic aperture radar (SAR), echoes are often modeled by incorporating time-varying acceleration [5], [6]. Target acceleration was shown to affect the SAR ground moving-target indication in [7] and [8], where compensation techniques were also examined. IFR can be estimated by using a polynomial Fourier transform [9]. The resulting estimator, however, requires a computationally intensive multidimensional search [9]. This motivated later efforts to search for more efficient solutions. A notable example is the cubic phase function (CPF) based estimator [3], which requires only a one-dimensional search. The CPF was originally introduced to estimate the IFR of a quadratic FM signal. Extension of the CPF led to the high-order phase function (HPF) [10], which can be used to estimate the IFR of a high-order PPS. The asymptotic performance of the CPF-based IFR estimate for the quadratic FM signal was derived in [10]. However, similar analysis for the HPF-based IFR estimator of a general PPS is unavailable.

In this paper, a unified analysis of the HPF-based IFR estimator for a PPS with an arbitrary order is presented. The asymptotic bias and variance of the HPF-based IFR estimate are derived in closed-form at high signal-to-noise ratio (SNR) by using a first-order perturbation analysis. It is shown that the HPF-based IFR estimator is asymptotically unbiased and its asymptotic variance is a function of the SNR, time and the HPF coefficients (see Section III for an explanation). Our results are consistent with that derived in [3] and [10] for the case of $p = 3$. Furthermore, since multiple forms of the HPF exist for the analysis of a given PPS, our results can be used to predict their performance and provide guideline on how to choose a proper HPF for the problem at hand. On the other hand, to establish a performance benchmark for all (asymptotically) unbiased IFR estimators, the Cramér–Rao bounds (CRBs) for IFR estimation, in both exact and asymptotic forms, are presented in closed-form. The CRB shows a dependence on the PPS order, the number of samples, time and SNR. Performance comparison between the HPF-based estimators and the high-order ambiguity function (HAF)-based method [11] is also presented.

The rest of this paper is organized as follows. The HPF is first reviewed in Section II. Section III outlines the derived expressions for the asymptotic bias and mean-squared error (MSE). The CRB for IFR estimation is also derived. Section IV provides simulation results to verify our theoretical analysis. Finally, conclusions are provided in Section V.

II. High-Order Phase Function

For a pth-order PPS defined in (1), the HPF, specified by $H_q(t,\omega)$, was defined by using a high-order nonlinear kernel $K_q(t,\tau)$ as [10]

$$K_q(t,\tau) = \prod_{l=1}^{q/2}\left[s(t+d_l\tau)s(t-d_l\tau)\right]^{(r_l)}$$
$$H_q(t,\omega) = \int_{-\infty}^{+\infty} K_q(t,\tau)e^{-j\omega\tau^2}d\tau \tag{3}$$

where $\mathbf{d} \triangleq \{d_1, d_2, \ldots, d_{q/2}\}$ denotes a set of lag-coefficients, $\mathbf{r} \triangleq \{r_1, r_2, \ldots, r_{q/2}\}$ is used to impose complex conjugation if $r_i = -1$, and ω denotes the index in the IFR domain. From (3), it is seen that the HPF has a qth-order nonlinearity due to the $q/2$ consecutive bilinear transformations. If $q = 2$, $d_1 = 1$ and $r_1 = 1$, the $H_2(t,\omega)$ reduces to the CPF in [3].

In the noisy-free case, assume the kernel is selected such that

$$K_q(t,\tau) = A^q e^{j\tau^2\Omega(t)+j\varsigma} \tag{4}$$

where ς is a term independent of τ, the squared magnitude of the HPF is centered on the IFR due to the match filtering in (3). To meet (4), the HPF coefficients should satisfy [12]

$$\sum_{l=1}^{q/2} r_l d_l^2 = 1$$
$$\sum_{l=1}^{q/2} r_l d_l^m = 0, \text{ for even values of } m: 4 \le m \le p. \tag{5}$$

Manuscript received February 16, 2009; accepted September 24, 2009. First published October 20, 2009; current version published March 10, 2010. The associate editor coordinating the review of this manuscript and approving it for publication was Dr. Chong-Meng Samson See. This work was supported in part by the Air Force Research Laboratory (AFRL) under Contract FA8750-05-2-0001, by the Air Force Office of Scientific Research (AFOSR) under Grant FA9550-09-1-0310, and by the National Natural Science Foundation of China under Grant 60802062.

P. Wang and H. Li are with the Department of Electrical and Computer Engineering, Stevens Institute of Technology, Hoboken, NJ 07030 USA (e-mail: pwang4@stevens.edu; hli@stevens.edu).

I. Djurović is with the Electrical Engineering Department, University of Montenegro, Podgorica 81000, Montenegro (e-mail: igordj@cg.ac.yu).

B. Himed is with the AFRL/RYRT, Dayton, OH 45433 USA (e-mail: Braham.Himed@wpafb.af.mil).

Digital Object Identifier 10.1109/TSP.2009.2034939

Therefore, for any given time, e.g., $t = t_s$, the IFR $\Omega(t_s)$ can be estimated by searching for the maximum of $|H_q(t_s, \omega)|^2$ over ω.

For a given PPS, there may exist more than one real solution to the set of equations in (5). For example of a quadratic FM signal ($p = 3$), we have at least two choices satisfying (5)

$$H_2(t,\omega) = \int_{-\infty}^{+\infty} s(t+\tau)s(t-\tau)e^{-j\omega\tau^2}d\tau, \quad (6)$$

$$H_4(t,\omega) = \int_{-\infty}^{+\infty} s^2\left(t+\frac{\sqrt{2}}{2}\tau\right)s^2\left(t-\frac{\sqrt{2}}{2}\tau\right)e^{-j\omega\tau^2}d\tau. \quad (7)$$

One immediate question arising from the earlier discussion is the choice of the solution for the problem at hand. A natural choice to select a proper form of HPF is the performance of the estimator including the bias, the MSE, and the SNR threshold, which will be discussed later.

III. Performance of the HPF-Based IFR Estimator

Consider a noise-corrupted PPS

$$x(n) = Ae^{j\sum_{i=0}^{p} a_i n^i} + v(n), \quad n = 0, 1, \ldots, N-1 \quad (8)$$

where $x(n)$ denotes the nth sample of the noisy observations, $v(n)$ is an additive complex white Gaussian noise with zero mean and variance σ^2, and N is the number of samples. It should be noted that, while condition (5) ensures the unbiased IFR estimate in the absence of noise, the unbiased property does not automatically carry over the case with observation noise.

The discrete HPF [cf. (3)] for the noisy PPS can be decoupled to

$$H_x(n,\omega) = \sum_{m=-M}^{M} \left[K_s(n,m) + K_v(n,m)\right] e^{-j\omega m^2} \quad (9)$$

where $K_s(n,m)$ and $K_v(n,m)$ represent the signal and noise components, respectively, $2M+1$ is the length of a two-sided window. For simplicity, we use ω in both continuous and discrete cases.

Appendix I shows that, at high SNR, the signal component $K_s(n,m)$ and the noise component $K_v(n,m)$ can be approximated by ignoring the high-order noise terms [13]

$$K_s(n,m) = \prod_{i=1}^{L} \left[s(n+d_i m)s(n-d_i m)\right]^{(r_i)k_i}$$

$$K_v(n,m) \approx K_s(n,m)\left(\sum_{i=1}^{L} k_i \left[\frac{v^{(r_i)}(n+d_i m)}{s^{(r_i)}(n+d_i m)} + \frac{v^{(r_i)}(n-d_i m)}{s^{(r_i)}(n-d_i m)}\right]\right). \quad (10)$$

where L is the number of distinct HPF coefficient pairs (d_i, r_i), k_i is the multiplicity of the ith HPF coefficient pair (d_i, r_i), and $\sum_{i=1}^{L} k_i = q/2$. From (10), it is seen that $K_s(n,m)$ contains only signal-related terms and therefore is deterministic, whereas $K_v(n,m)$ includes interacting signal-and-noise terms which are random. More specifically, $K_v(n,m)$ acts like a random perturbation which moves the maximum of the HPF, denoted as $\omega_0 = \Omega(n)$, by a random amount $\delta\omega$, which results in a deviated IFR estimate $\hat{\omega} = \omega_0 + \delta\omega$. The performance analysis is to quantify the first- and second-order statistics, i.e., the bias and variance, of the random error $\delta\omega$. A first-order perturbation analysis [14], which is repeated in Appendix II, is utilized. A detailed analysis of the random estimate error $\delta\omega$ using the first-order perturbation is presented in Appendix III, and the results are summarized as follows.

A. Asymptotic Bias and Variance of the HPF-Based Estimator

Proposition 1: For a pth-order noisy PPS, the asymptotic bias and variance of the HPF-based IFR estimator at high SNR are given by

$$E\{\delta\omega\} = 0$$

$$E\left\{(\delta\omega)^2\right\} = \frac{90\sum_{i=1}^{L} {k_i}^2}{\mathrm{SNR}M(M+1)(2M+3)(4M^2-1)} \quad (11)$$

where the SNR is defined as A^2/σ^2.

From *Proposition 1*, the HPF-based IFR estimator is asymptotically unbiased, and the variance of the estimation error, which is also the MSE in this case, is independent of the phase parameter $\{a_i\}_{i=0}^{p}$. On one hand, the MSE is proportional to the sum of the squared multiplicity of the HPF coefficients. On the other hand, the asymptotic MSE is inversely proportional to the SNR and M^5. The larger the window length, the lower the MSE. As such, for a given SNR and time n, the minimum MSE is achieved by using the maximum window length, which leads to the following proposition.

Proposition 2: For a fixed SNR and N, the minimum MSE of the HPF-based IFR estimator at time n is given by

$$E\left\{(\delta\omega)^2\right\} \approx \frac{45\sum_{i=1}^{L} {k_i}^2}{4\mathrm{SNR}M_{\max}^5(n,N,\mathbf{d})} \quad (12)$$

where the maximum window length at time n is given by

$$M_{\max}(n,N,\mathbf{d}) = \left\lfloor \frac{\min\{n, N-1-n\}}{\max\{\mathbf{d}\}} \right\rfloor \quad (13)$$

with $\lfloor\cdot\rfloor$ denotes the floor function, since $0 \le n \pm \max\{\mathbf{d}\} M_{\max} \le N-1$. From *Proposition 2*, the minimum MSE of the IFR estimator at time n is determined by the SNR, the number of samples, time instant, and the HPF coefficients $\mathbf{d}$. Note that the MSE is also a function of the HPF order q through L and k_i since $\sum_{i=1}^{L} k_i = q/2$, and is further dependent on the PPS order p due to (5).

B. CRB for IFR Estimation

The achievable accuracy of any (asymptotically) unbiased IFR estimator can be identified by means of the CRB. To this end, we derive the CRBs for IFR estimation in both exact and asymptotic forms.

1) Exact CRB: The CRB for estimating the phase parameter $\mathbf{a} \triangleq [a_0, a_1, \ldots, a_p]^T$ was carried out in [15]. Of interest to us is the CRB for IFR estimation, not for the phase parameter $\mathbf{a}$. Note, however, that the IFR of the PPS is a function of $\mathbf{a}$ and time n as $\Omega(n) = \mathbf{a}^T\mathbf{t}$, where $\mathbf{t} \triangleq \left[0, 0, 2, \ldots, p(p-1)n^{p-2}\right]^T$. By applying the transformation rule for the CRB (see [16, Appendix 3B]) and noting that the above function is a $(p+1)$-dimensional-to-scalar transformation, we have

$$\mathrm{var}(\hat{\omega}) \ge \frac{\sigma^2}{2A^2}\mathbf{t}\mathbf{H}_{p+1}^{-1}\mathbf{t}^T \quad (14)$$

where $\mathbf{H}_{p+1}$ is defined in [15, (18)]. With results on the inverse of $\mathbf{H}_{p+1}$ (see [15, (22)–(33)]), (14) can further be expressed

$$\mathrm{var}(\hat{\omega}) \ge \frac{\sigma^2}{2A^2N}\mathbf{t}\mathbf{E}_{p+1}^{-1}\mathbf{B}_{p+1}\mathbf{E}_{p+1}^{-1}\mathbf{t}^T \quad (15)$$

where $\mathbf{E}_{p+1}$ and $\mathbf{B}_{p+1}$ are defined in [15, (24) and (32)]. From (15), it is not clear how the coefficients (e.g., p, n, N) affect the CRB. In the following, we show how the CRB depends on these coefficients under the assumption of large samples.

TABLE I
VALUES OF $C_p(k)$ FOR THE PPS WITH ORDER $p \leq 4$

p	$k=0$	$k=1$	$k=2$	$k=3$	$k=4$
2	720				
3	25920	-100800	100800		
4	317520	-2822400	9172800	-12700800	6350400

2) Asymptotic CRB for Large N: For large N (i.e., $N \gg p$), noting that

$$\frac{1}{\iota+\kappa+1} \gg \frac{(p+1)^2}{2N(\iota+1)(\kappa+1)} - \frac{1}{2N}, \quad 2 \leq \iota, \kappa \leq p, \quad N \gg p$$

in the expression of $\mathbf{B}_{p+1}$, we derive an asymptotic CRB.

Proposition 3: For a noisy pth-order PPS, the asymptotic variance of any unbiased IFR estimator is bounded by

$$\mathrm{var}\,(\hat{\omega}) \geq \frac{1}{2\mathrm{SNR}} \sum_{k=0}^{2p-4} C_p(k) \frac{n^k}{N^{(k+5)}} \tag{16}$$

where

$$C_p(k) = \sum_{\substack{2 \leq \iota, \kappa \leq p \\ \iota+\kappa-4=k}} c_p(\iota,\kappa) \tag{17}$$

with

$$c_p(\iota,\kappa) = (-1)^{\iota+\kappa} \frac{\iota\kappa(\iota-1)(\kappa-1)(p+\iota+1)(p+\kappa+1)}{\iota+\kappa+1} \times \binom{p+\iota}{\iota}\binom{p}{\iota}\binom{p+\kappa}{\kappa}\binom{p}{\kappa}.$$

Remark: The above CRB is for the asymmetric sampling case $n = 0, \ldots, N-1$. It can be extended to the symmetric sampling case $n = -(N-1)/2, \ldots, (N-1)/2$. According to [17], it can be shown that the asymptotic CRB for IFR estimation in the asymmetric sampling case is

$$\mathrm{var}\,(\hat{\omega}) \geq \frac{1}{2\mathrm{SNR}} \sum_{k=0}^{2p-4} C_p(k) \frac{\left(n+\frac{N-1}{2}\right)^k}{N^{(k+5)}}. \tag{18}$$

Note that the coefficients $C_p(k)$ are a function of p only and hence can be computed in advance for any given PPS order. Table I shows the values of $C_p(k)$ for the PPS with order $p \leq 4$. Moreover, the asymptotic CRB in (16) is a $(2p-4)$th-order polynomial in n with coefficient $C_p(k)/\left(2\mathrm{SNR}N^{k+5}\right)$ for the kth item in n. This polynomial phenomenon is analogous to the polynomial structure of the IFR in n (see (2)) where the kth term n^k is associated with a^{k+2} whose CRB is inversely proportional to the SNR and N^{2k+5}.

The accuracy of approximating (15) with (16) is examined at the middle point of observations in the cases of $p = 4$ and $p = 6$ when $\mathrm{SNR} = 10$ dB in Fig. 1. It is seen that our large sample approximation works fine even for small N. For $N \geq 100$, the approximation makes no difference between the two CRBs.

C. Examples

In general, the above results on the variance of the HPF-based IFR estimate and the CRB for IFR estimation are valid for any PPS with an order p. Nevertheless, links to two simple cases of $p = 2$ and $p = 3$ are useful to illustrate our analytical results.

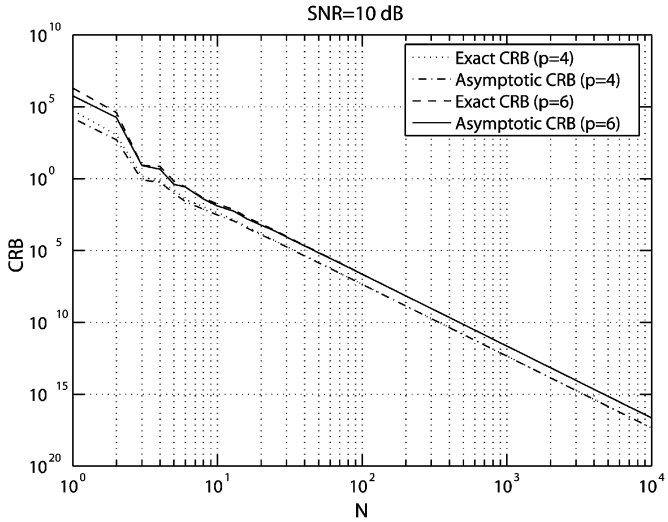

Fig. 1. Exact and asymptotic CRBs versus the number of samples N.

Linear FM Signal ($p = 2$): The IFR reduces to $\Omega(n) = 2a_2$, and the CRB for IFR estimation is

$$\mathrm{CRB}\,\{\Omega\} = \frac{360}{N^5\mathrm{SNR}}. \tag{19}$$

Using the transformation rule of the CRB [16, Section 3.6], this result is effectively the same as the CRB for a_2 of the linear FM signal (see [14, (33)]) by a factor of 4 since $\Omega(n) = 2a_2$.

When H_2 in (6) is used, the MSE of the IFR estimate in (11) at the middle point from (12) is

$$E\left\{(\delta\omega)^2\right\} \approx \frac{360}{N^5\mathrm{SNR}} \tag{20}$$

which is consistent with the MSE of the H_2-based a_2 estimate at the middle point by a factor of 4 [12, Appendix-A].

Quadratic FM Signal ($p = 3$): From (16), the CRB for IFR estimation is a function of n, SNR, and N

$$\mathrm{CRB}\,\{\Omega\} = \frac{12960}{N^5\mathrm{SNR}} - \frac{50400}{N^6\mathrm{SNR}}n + \frac{50400}{N^7\mathrm{SNR}}n^2. \tag{21}$$

As discussed earlier, the CRB is a second-order polynomial in n.

As shown in [10], H_2 can be used to estimate the IFR of the quadratic FM signal. In this case, the MSE in (11) reduces to

$$E\left\{(\delta\omega)^2\right\} \approx \frac{45}{4M^5\mathrm{SNR}}. \tag{22}$$

To connect our results to [10], we notice that the maximum window length of H_2 at time n is $M_{\max} = N/2 - |n|$ for the case $-(N-1)/2 \leq n \pm m \leq (N-1)/2$, as considered in [10]. Therefore, the minimum MSE of the H_2-based IFR estimate at n is

$$E\left\{(\delta\omega)^2\right\} \approx \frac{45}{4\left(\frac{N}{2}-|n|\right)^5\mathrm{SNR}} \tag{23}$$

which coincides with [10, (40)] at high SNR.

IV. SIMULATION RESULTS

In the following, we consider two numerical examples to verify our analytical results. All simulated results are based on 300 Monte Carlo simulations. For the HPF-based methods, interpolation is used whenever the lag-coefficient is not an integer.

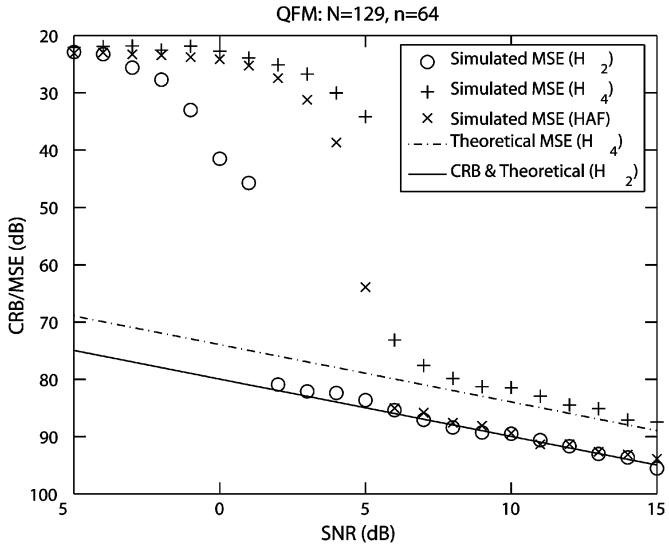

Fig. 2. MSEs of the H_2, H_4 and the HAF versus SNR for a quadratic FM signal.

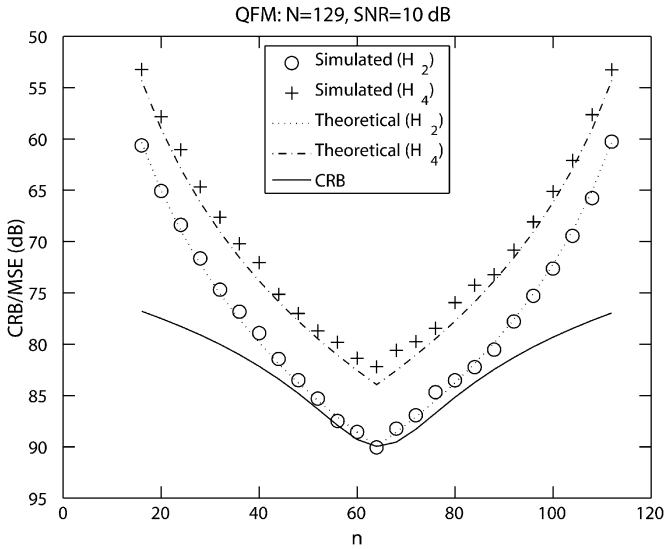

Fig. 3. MSEs of various HPFs versus time n for a quadratic FM signal.

A. Quadratic FM Signal

For a quadratic FM signal, both H_2 and H_4 can be applied to estimate the IFR. According to Proposition 1, the asymptotic MSEs for both estimates are

$$E\left\{(\delta\omega)^2\right\}_{H_2} \approx \frac{45}{4M^5\mathrm{SNR}}$$
$$E\left\{(\delta\omega)^2\right\}_{H_4} \approx \frac{45}{M^5\mathrm{SNR}}.$$

To verify our analytical results, a quadratic FM signal with parameters $A=1, (a_0,a_1,a_2,a_3)=\left(1,\pi/8,5\times10^{-3},10^{-5}\right)$, and $N=129$ is generated. Fig. 2 shows the simulated MSE at $n=64$ (i.e., the middle point of observations) by using H_2, H_4 and the HAF when the SNR varies from -5 dB to 15 dB. The length of window is $M=64$. From this figure, we have the following observations:

1) At high SNR, the simulated MSEs for both H_2 and H_4 agree with their own theoretical results. Note that the theoretical and simulated MSEs of the H_2 attain the CRB when the SNR is above 1 dB. The MSEs of the H_4-based estimate are about four times higher than the H_2-based and HAF-based MSEs when the SNR is greater than 6 dB.
2) The H_4 and the HAF show a higher SNR threshold than the H_2 because the former two involve a fourth-order nonlinearity while the H_2-based method has only a second-order nonlinearity. In this example, the SNR threshold for the H_4 and the HAF is about 6 dB, whereas the H_2 exhibits a threshold at around 2 dB. Note that nonlinear estimators usually exhibit a threshold effect (see [16, Ch. 7]).

The variation of the MSE as a function of n is shown in Fig. 3 when $N=129$ and $\mathrm{SNR}=10$ dB. At each time point n, we use the window length $M=\min\{n,N-1-n\}$. Both the MSE and CRB are seen to be symmetric with respect to the middle point $n=64$. The numerical results are seen to agree with the theoretical results. Again, the H_2-based estimator shows lower MSEs than those of the H_4-based estimator. In general, for a quadratic FM signal, the H_2-based estimator provides the best performance in terms of MSEs and the SNR threshold among various HPFs.

B. Cubic FM Signal

For a cubic FM signal ($p=4$), the minimum HPF order is $q=6$ due to (5). By minimizing the theoretical MSE in *Proposition 2* with subject to (5), we can numerically determine the sixth-order HPF with the minimum MSE as H_6 with $\mathbf{r}=(1,1,-1)$ and $\mathbf{d}=(1.2646,1.3544,1.5600)$. For comparison purposes, we also consider two other HPFs: (1) H_6' with $\mathbf{r}=(1,1,-1)$ and $\mathbf{d}=(1.0875,1.9333,1.9800)$, and (2) H_8 with $\mathbf{r}=(1,1,-1,-1)$ and $\mathbf{d}=(1.4759,2.9432,2.9800,0.9800)$. Their theoretical MSEs can easily be obtained from *Proposition 2* and will be compared in the following simulations.

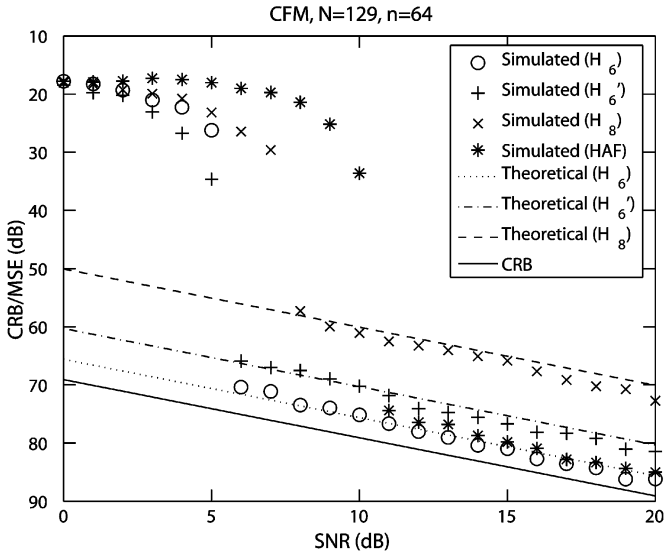

Fig. 4. MSEs of various HPFs and the HAF versus SNR for a cubic FM signal.

To verify our analytical results, a cubic FM signal with parameters $A=1$, $(a_0,a_1,a_2,a_3,a_4)=\left(1,\pi/8,3\times10^{-4},2.5\times10^{-7},10^{-10}\right)$, and $N=129$ is generated. Fig. 4 shows the theoretical and simulated MSEs for the three HPFs and the HAF as a function of the SNR when the IFR is estimated at $n=64$. The results verify again that our theoretical MSEs agree well with the simulations for the H_6, H_6' and H_8-based methods at high SNR. We note that the H_6-based estimator provides the minimum MSE among the three. Moreover, the two sixth-order HPF H_6 and H_6' show a lower SNR threshold than that of the eighth-order HPF H_8. Comparison with the HAF-based estimator shows that the HAF-based estimator

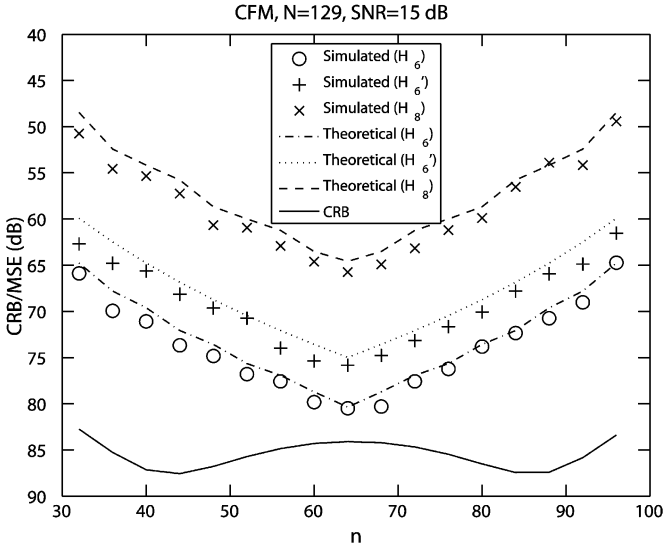

Fig. 5. MSEs of various HPFs versus time n for a cubic FM signal.

can generate good performance at SNRs above 11 dB, but its SNR threshold is higher than the HPF-based methods.

Fig. 5 plots the MSEs of the three HPF-based estimators with the maximum window length $M_{\max}$ in (13) versus time n when $\mathrm{SNR} = 15$ dB. It is observed that, even at the middle point, the MSE of the three IFR estimators cannot reach the CRB. Once again, the simulated MSEs match the theoretical results. From Figs. 4 and 5, it is seen that the best HPF for the cubic FM signal is H_6 in terms of either the MSEs or the SNR threshold.

V. Conclusion

This paper has presented a generalized performance analysis of the HPF-based IFR estimators in terms of their asymptotic bias and MSE for the estimation of polynomial phase signals with an arbitrary order. The results show that the MSE of the IFR estimate is proportional to the sum of squared multiplicity of the HPF coefficients, and inversely proportional to the SNR and the window length. Both exact and asymptotic CRBs for the IFR estimation have been established. Two examples have been provided to show that our results are consistent with the existing results for the cases of $p = 2$ and $p = 3$. Numerical examples have been given to verify the analytical results.

Appendix I
Approximation of $K_x(n,m)$ at High SNR

By applying the HPF to the above noisy PPS signal, the nonlinear kernel of the HPF in discrete form can be expressed as

$$K_x(n,m) = \prod_{i=1}^{L} [s(n+d_i m) + v(n+d_i m)]^{(r_i)k_i} \times [s(n-d_i m) + v(n-d_i m)]^{(r_i)k_i} \quad (24)$$

where L is the number of different coefficients d_i and r_i, k_i is the multiplicity of the coefficients d_i and r_i, and $\sum_{i=1}^{L} k_i = q/2$.

Using the binomial expansion

$$[s(n+d_i m) + v(n+d_i m)]^{(r_i)k_i} = \sum_{\ell=0}^{k_i} \binom{k_i}{\ell} v^{(r_i)\ell}(n+d_i m) s^{(r_i)[k_i-\ell]}(n+d_i m) \quad (25)$$

and a similar expansion for $[s(n-d_i m) + v(n-d_i m)]^{(r_i)k_i}$, we can rewrite (24) as follows:

$$\begin{aligned} K_x(n,m) &= \prod_{i=1}^{L} s^{(r_i)k_i}(n+d_i m) s^{(r_i)k_i}(n-d_i m) \\ &\quad \times \left[\sum_{\ell_1=0}^{k_i} \sum_{\ell_2=0}^{k_i} \binom{k_i}{\ell_1} \binom{k_i}{\ell_2} v^{\ell_1}(n+d_i m) \right. \\ &\quad \left. \times v^{\ell_2}(n-d_i m) s^{-\ell_1}(n+d_i m) s^{-\ell_2}(n-d_i m) \right]^{(r_i)} \\ &\approx \prod_{i=1}^{L} s^{(r_i)k_i}(n+d_i m) s^{(r_i)k_i}(n-d_i m) \\ &\quad \times \left[1 + k_i v(n-d_i m) s^{-1}(n-d_i m) \right. \\ &\quad \left. + k_i v(n+d_i m) s^{-1}(n+d_i m) \right]^{(r_i)} \end{aligned} \quad (26)$$

where the approximation is due to the high SNR assumption which allows us to ignore the high-order noise terms. Decomposing (26) into signal-only terms and noise-related terms, we have

$$\begin{aligned} K_x(n,m) &\approx \left\{ \prod_{i=1}^{L} \left[s^{k_i}(t+d_i\tau) s^{k_i}(t-d_i\tau) \right]^{(r_i)} \right\} \\ &\quad \times \left\{ 1 + \sum_{i=1}^{L} k_i \left[v(n-d_i m) s^{-1}(n-d_i m) \right. \right. \\ &\quad \left. \left. + v(n+d_i m) s^{-1}(n+d_i m) \right]^{(r_i)} \right\} \\ &= K_s(n,m) + K_s(n,m) \\ &\quad \times \sum_{i=1}^{L} k_i \left[v(n+d_i m) s^{-1}(n+d_i m) \right. \\ &\quad \left. + v(n-d_i m) s^{-1}(n-d_i m) \right]^{(r_i)} \end{aligned}$$

which is (10).

Appendix II
First-Order Perturbation Method

The basic principle of the first-order permutation method is shown as follows. Assume that $g_N(\omega)$ is a complex function depending on a real variable ω and on an integer N. The squared-magnitude of $g_N(\omega)$ has a global maximum at $\omega = \omega_0$. Suppose a random function $\delta g_N(\omega)$ moves the global maximum of $g_N(\omega)$ from the nominal ω_0 by $\delta\omega$, the first-order approximation for $\delta\omega$ is $\delta\omega \approx -\beta/\alpha$ [14], where

$$\alpha = 2\Re\left\{ g_N(\omega_0) \frac{\partial^2 g_N^*(\omega_0)}{\partial\omega^2} + \frac{\partial g_N(\omega_0)}{\partial\omega} \frac{\partial g_N^*(\omega_0)}{\partial\omega} \right\} \quad (27)$$

and

$$\beta = 2\Re\left\{ g_N(\omega_0) \frac{\partial \delta g_N^*(\omega_0)}{\partial\omega} + \frac{\partial g_N(\omega_0)}{\partial\omega} \delta g_N^*(\omega_0) \right\} \quad (28)$$

where $\Re(\cdot)$ represents the real part of $(\cdot)$. The mean-square value of $\delta\omega$ is given by

$$E\{(\delta\omega)^2\} \approx \frac{E\{\beta^2\}}{\alpha^2} \quad (29)$$

where $E\{\cdot\}$ denotes the expectation.

APPENDIX III
ASYMPTOTIC ANALYSIS OF THE HPF-BASED ESTIMATOR

The HPF of a noise-free PPS $s(n)$ is

$$H_s(n,\omega)=\sum_{m=-M}^{M}K_s(n,m)e^{-j\omega m^2}. \tag{30}$$

By choosing the HPF coefficients according to *Proposition 1*, the HPF attains the maximum at $\omega_0=\Omega(n)$.

To derive its asymptotic MSE of the HPF-based IFR estimate, we first determine the complex function $g_N(\omega)$ and its random perturbation $\delta g_N(\omega)$ for a specific n. According to the results in Appendix I, $g_N(\omega)$ and $\delta g_N(\omega)$ can be expressed as

$$\begin{aligned} g_N(\omega)&=\sum_{m=-M}^{M}K_s(n,m)e^{-j\omega m^2},\\ \delta g_N(\omega)&=\sum_{m=-M}^{M}K_v(n,m)e^{-j\omega m^2} \end{aligned} \tag{31}$$

where $K_v(n,m)$ is given in (10). For simplicity, we drop the index n in the above functions. Since

$$K_s(n,m)=A^q e^{j\left(\omega_0 m^2+\varsigma\right)} \tag{32}$$

the functions $g_N(\omega),\delta g_N(\omega)$, and their derivatives, evaluated at the global maximum $\omega_0=\Omega(n)$, are given by

$$\begin{aligned} g_N(\omega_0)&=A^q e^{j\varsigma}(2M+1)\\ \frac{\partial g_N(\omega_0)}{\partial\omega}&=-j\frac{A^q e^{j\varsigma}}{3}M(M+1)(2M+1),\\ \frac{\partial^2 g_N(\omega_0)}{\partial\omega^2}&=-\frac{A^q e^{j\varsigma}}{15}M(M+1)(2M+1)\\ &\quad\times\left(3M^2+3M-1\right),\\ \delta g_N^*(\omega_0)&=A^q e^{-j\varsigma}\sum_m z_{vs}(n,m),\\ \frac{\partial\delta g_N^*(\omega_0)}{\partial\omega}&=jA^q e^{-j\varsigma}\sum_m m^2 z_{vs}(n,m) \end{aligned}$$

where

$$\begin{aligned} z_{vs}(n,m)=\sum_{i=1}^{L}k_i\big[&v(n+d_im)s^{-1}(n+d_im)\\ &+v(n-d_im)s^{-1}(n-d_im)\big]^{(-r_i)} \end{aligned} \tag{33}$$

and $(\cdot)^{(-r_i)}$ means the conjugate of $(\cdot)^{(r_i)}$.

By inserting the above intermediate results into (27) and (28), we obtain

$$\begin{aligned} \alpha&=-\frac{2A^{2q}}{45}M(M+1)(2M-1)(2M+1)^2(2M+3),\\ \beta&=2A^{2q}(2M+1)\Im[\Gamma] \end{aligned} \tag{34}$$

where $\Im[\cdot]$ represents the imaginary part of $[\cdot]$ and

$$\Gamma=\sum_m\left(m^2-\frac{M(M+1)}{3}\right)z_{vs}(n,m). \tag{35}$$

Therefore, the first-order approximation of the perturbation on the maximum point $\delta\omega$ is

$$\delta\omega=\frac{45\Im[\Gamma]}{M(M+1)(2M-1)(2M+1)(2M+3)}. \tag{36}$$

Taking the expectation of (36) with respect to $v(n)$, we can verify, from (33) and (36), that $E\{z_{vs}(n,m)\}=0$, and, hence

$$E\{\delta\omega\}=0. \tag{37}$$

In other words, the estimator is asymptotically unbiased.

According to (29), we need to compute $E\left\{\beta^2\right\}$ in order to find the asymptotic variance. From (34)

$$E\left\{\beta^2\right\}=2A^{4q}(2M+1)^2\Re\left[E\{\Gamma\Gamma^*\}-E\{\Gamma\Gamma\}\right] \tag{38}$$

where we use the fact that

$$E\{\Im[x]\Im[y]\}=0.5\Re\left[E\{xy^*\}-E\{xy\}\right].$$

From (35), we have

$$\begin{aligned} E\{\Gamma\Gamma^*\}=&\sum_{m_1}\sum_{m_2}\left(m_1^2-\frac{M(M+1)}{3}\right)\left(m_2^2-\frac{M(M+1)}{3}\right)\\ &\times E\{z_{vs}(n,m_1)z_{vs}^*(n,m_2)\} \end{aligned} \tag{39}$$

$$\begin{aligned} E\{\Gamma\Gamma\}=&\sum_{m_1}\sum_{m_2}\left(m_1^2-\frac{M(M+1)}{3}\right)\left(m_2^2-\frac{M(M+1)}{3}\right)\\ &\times E\{z_{vs}(n,m_1)z_{vs}(n,m_2)\}. \end{aligned} \tag{40}$$

Using (41) to evaluate $E\{z_{vs}(n,m_1)z_{vs}^*(n,m_2)\}$ and $E\{z_{vs}(n,m_1)z_{vs}(n,m_2)\}$ results in

$$\begin{aligned} &E\{z_{vs}(n,m_1)z_{vs}^*(n,m_2)\}\\ &\quad\approx 2\sigma^2A^{-2}\sum_{i=1}^{L}(k_i)^2\delta(m_1\pm m_2)\\ &E\{z_{vs}(n,m_1)z_{vs}(n,m_2)\}\approx 0 \end{aligned}$$

where we used the fact that $d_i\neq d_j$ and $r_i\neq r_j$ if $i\neq j$. Inserting these intermediate results into (38)–(40) yields

$$\begin{aligned} E\left\{\beta^2\right\}=&\frac{8A^{4q-2}\sigma^2\sum_{i=1}^{n_1}(k_i)^2}{45}M(M+1)\\ &\times(2M-1)(2M+1)^3(2M+3). \end{aligned} \tag{41}$$

Combining (29), (34) and (41), the variance of $\delta\omega$ is

$$E\{(\delta\omega)^2\}=\frac{90\sum_{i=1}^{L}(k_i)^2}{\mathrm{SNR}M(M+1)(2M-1)(2M+1)(2M+3)}.$$

REFERENCES

[1] A. W. Rihaczek, *Principles of High-Resolution Radar*. New York: McGraw-Hill, 1969.

[2] B. Porat, *Digital Processing of Random Signals: Theory and Methods*. Englewood Cliffs, NJ: Prentice-Hall, 1994.

[3] P. O'Shea, "A new technique for estimating instantaneous frequency rate," *IEEE Signal Process. Lett.*, vol. 9, pp. 251–252, Aug. 2002.

[4] T. Abotzoglou, "Fast maximum likelihood joint estimation of frequency and frequency rate," *IEEE Trans. Aerosp. Electron. Syst.*, vol. 22, pp. 708–715, Nov. 1986.

[5] S. Barbarossa, A. Scaglione, and G. Giannakis, "Product high-order ambiguity function for mulit-component polynomial phase signal modeling," *IEEE Trans. Signal Process.*, vol. 46, no. 3, pp. 691–708, Mar. 1998.

[6] S. Barbarossa and A. Scaglione, "Autofocusing of SAR images based on the product high-order ambiguity function," *Proc. Inst. Electr. Eng.—Radar Sonar Navig.*, vol. 145, no. 5, pp. 269–273, Oct. 1998.

[7] J. J. Sharma, C. H. Gierull, and M. J. Collins, "The influence of target acceleration on velocity estimation in dual-channel SAR-GMTI," *IEEE Trans. Geosci. Remote Sens.*, vol. 44, no. 1, pp. 134–147, Jan. 2006.

[8] J. J. Sharma, C. H. Gierull, and M. J. Collins, "Compensating the effects of target acceleration in dual-channel SAR-GMTI," *Proc. Inst. Electr. Eng.—Radar Sonar Navig.*, vol. 153, no. 1, pp. 53–62, Feb. 2006.

[9] V. Katkovnik, "Nonparametric estimation of instantaneous frequency," *IEEE Trans. Inf. Theory*, vol. 43, no. 1, pp. 183–189, Jan. 1997.

[10] P. O'Shea, "A fast algorithm for estimating the parameters of a quadratic FM signal," *IEEE Trans. Signal Process.*, vol. 52, no. 2, pp. 385–393, Feb. 2004.

[11] B. Porat and B. Friedlander, "Asymptotic statistical analysis of the high-order ambiguity function for parameter estimation of polynomial-phase signals," *IEEE Trans. Inf. Theory*, vol. 42, no. 3, pp. 995–1001, May 1996.
[12] P. Wang, I. Djurović, and J. Yang, "Generalized high-order phase function for parameter estimation of polynomial phase signal," *IEEE Trans. Signal Process.*, vol. 56, no. 7, pp. 3023–3028, Jul. 2008.
[13] B. Barkat and B. Boashash, "Instantaneous frequency estimation of polynomial FM signals using the peak of the PWVD: Statistical performance in the presence of additive Gaussian noise," *IEEE Trans. Signal Process.*, vol. 47, no. 9, pp. 2480–2490, Sep. 1999.
[14] S. Peleg and B. Porat, "Linear FM signal parameter estimation from discrete-time observations," *IEEE Trans. Aerosp. Electron. Syst.*, vol. 27, pp. 607–614, Jul. 1991.
[15] S. Peleg and B. Porat, "The Cramer-Rao lower bound for signals with constant amplitude and polynomial phase," *IEEE Trans. Signal Process.*, vol. 39, no. 3, pp. 749–752, Mar. 1991.
[16] S. M. Kay, *Fundamental of Statistical Signal Processing: Estimation Theory*. Upper Saddle River, NJ: Prentice-Hall, 1998.
[17] B. Ristic and B. Boashash, "Comments on the Cramer-Rao lower bounds for signals with constant amplitude and polynomial phase," *IEEE Trans. Signal Process.*, vol. 46, no. 6, pp. 1708–1709, Jun. 1998.

Range-Doppler Imaging via Forward-Backward Sparse Bayesian Learning

Xing Tan and Jian Li

***Abstract*—We consider range-Doppler imaging via transmitting a train of probing pulses as in radar and active sonar. We show that range-Doppler imaging can be formulated as a sparse signal recovery problem and that we can use an expectation maximization based sparse Bayesian learning (EM-SBL) algorithm to achieve high resolution imaging. We also reduce the complexity of EM-SBL significantly by using an efficient forward-backward algorithm in the E step of the EM algorithm.**

***Index Terms*—Forward-backward algorithm, radar imaging, Range-Doppler imaging, sparse Bayesian learning, super resolution.**

I. Introduction

In radar and active sonar applications, range-Doppler images of a scene can be obtained via transmitting a long probing pulse consisting of a train of modulated subpulses towards the scene of interest. This technique is often called pulse compression (see, e.g., [1]–[4]). Pulse compression radar and sonar have high range resolution and low instantaneous power because of its large time-bandwidth product, meaning that they can have both long pulse duration and large bandwidth at the same time. In [2], a data-independent instrumental variable (IV) filter was proposed for range-Doppler imaging. However, due to the use of only one probing pulse, the Doppler resolution of the range-Doppler image obtained by the IV filter in [2] is poor. To achieve higher Doppler resolution, the authors in [5] utilized multiple probing pulses, each consisting of a sequence of modulated subpulses, for range-Doppler imaging. Both the data-independent IV filter and the data-adaptive iterative adaptive approach (IAA) were considered in [5]. IAA was shown to have higher Doppler resolution than the IV filter at the cost of higher computational complexity. However, IAA does not provide the *a posteriori* probability density function (pdf) of the target's parameters, which is useful for target detection.

We consider herein a Bayesian method for range-Doppler imaging. The proposed method not only gives estimates for the target's parameters but also provides the *a posteriori* pdf of the target's parameters. The proposed Bayesian method is based on a two-stage Bayesian model (see, e.g., [6]). In [6], the hyper-parameters in the Bayesian model were estimated by a type-II maximum-likelihood (ML) method. The type-II ML method was solved by an expectation maximization (EM) based sparse Bayesian learning (SBL) approach, to which we refer as EM-SBL. We adopt EM-SBL for range-Doppler imaging herein. The main contribution of this correspondence is to reduce the complexity of EM-SBL by first transforming the Bayesian model into a hidden Markov model and then making use of an efficient forward-backward algorithm. We prove that the forward and backward densities in the forward-backward algorithm are Gaussian pdfs and hence, we only need to update their means and variances during the iterations. We refer to the so-obtained method as the forward-backward sparse Bayesian learning (FB-SBL) approach. Compared to EM-SBL, FB-SBL performs similarly but is much faster.

We denote vectors by boldface lowercase letters and matrices by boldface uppercase letters. The notations that we use throughout this paper are given in Table I.

TABLE I
NOTATIONS USED IN THE TEXT

$(\cdot)^T$	transpose of a vector or a matrix
$(\cdot)^H$	conjugate transpose of a vector or a matrix
$\boldsymbol{s}_{m:n}$	a column vector of the form $\left(\boldsymbol{s}_m^T, \boldsymbol{s}_{m+1}^T, \ldots, \boldsymbol{s}_n^T\right)^T$
$\mu(n)$	the nth element of the vector $\boldsymbol{\mu}$
$\Sigma(m,n)$	the (m,n)th entry of the matrix $\boldsymbol{\Sigma}$
$\boldsymbol{\mu}(m:n)$	a vector defined by $\left(\mu(m), \mu(m+1), \ldots, \mu(n)\right)^T$
$\boldsymbol{\Sigma}(k:l, m:n)$	a matrix defined by $\begin{pmatrix} \Sigma(k,m) & \ldots & \Sigma(k,n) \\ \vdots & & \vdots \\ \Sigma(l,m) & \ldots & \Sigma(l,n) \end{pmatrix}$
$\mathrm{diag}\{\boldsymbol{v}\}$	a diagonal matrix whose diagonal entries are the elements of the vector $\boldsymbol{v}$

II. Problem Formulation

We assume that a train of P probing pulses (with pulse repetition frequency f_r) is transmitted towards the scene of interest. Each probing pulse is a sequence of complex-valued subpulses $(c_0, c_1, \ldots, c_{M-1})$. Let the range of interest be divided into N range bins and the Doppler frequency shift interval of interest be divided into Q Doppler bins (denoted as $f_1, f_2, \ldots, f_Q$). Define the Doppler phase shift $\omega_q \triangleq 2\pi f_q / B$, where B is the bandwidth of the subpulses. The target

Manuscript received March 24, 2009; accepted October 20, 2009. First published December 01, 2009; current version published March 10, 2010. The associate editor coordinating the review of this manuscript and approving it for publication was Dr. Daniel P. Palomar. This material is based on research sponsored in part by the Office of Naval Research under Grant N00014-09-1-0211, the U. S. Army Research Laboratory and the U. S. Army Research Office under Contract/Grant W911NF-07-1-0450, the National Science Foundation (NSF) under Grant ECCS-0729727 and the Komen Breast Cancer Foundation under Grant BCTR0707587. The views and conclusions contained herein are those of the authors and should not be interpreted as necessarily representing the official policies or endorsements, either expressed or implied, of the U.S. Government. The U.S. Government is authorized to reproduce and distribute reprints for Governmental purposes notwithstanding any copyright notation thereon.

The authors are with the Department of Electrical and Computer Engineering, University of Florida, Gainesville, FL 32611-6130 USA (e-mail: tanxing@ufl.edu; li@dsp.ufl.edu).

Color versions of one or more of the figures in this paper are available online at http://ieeexplore.ieee.org.

Digital Object Identifier 10.1109/TSP.2009.2037667